Published in final edited form as:
Hum Mutat. 2011 June ; 32(6): 598–609. doi:10.1002/humu.21475.

COL1 C-propeptide Cleavage Site Mutations Cause High Bone Mass Osteogenesis Imperfecta

Katarina Lindahl[1,§], **Aileen M. Barnes**[2,§], **Nadja Fratzl-Zelman**[3], **Michael P. Whyte**[4], **Theresa E. Hefferan**[5], **Elena Makareeva**[6], **Marina Brusel**[7], **Michael J. Yaszemski**[5], **Carl-Johan Rubin**[1], **Andreas Kindmark**[1], **Paul Roschger**[3], **Klaus Klaushofer**[3], **William H. McAlister**[4], **Steven Mumm**[4], **Sergey Leikin**[6], **Efrat Kessler**[7], **Adele L. Boskey**[8], **Östen Ljunggren**[1], and **Joan C. Marini**[2]

[1] Department of Medical Sciences, Uppsala University, Uppsala, Sweden

[2] Bone and Extracellular Matrix Branch, *Eunice Kennedy Shriver* National Institute of Child Health and Human Development, National Institutes of Health, Bethesda, MD, USA

[3] Ludwig Boltzmann Institute of Osteology at the Hanusch Hospital of WGKK and AUVA Trauma Centre Meidling, 1st Medical Department, Hanusch Hospital, A-1140, Vienna, Austria

[4] Shriners Hospital for Children, and Washington University School of Medicine, St. Louis, MO, USA

[5] Department of Orthopedics, Mayo Clinic, Rochester, MN, USA

[6] Section on Physical Biochemistry, *Eunice Kennedy Shriver* National Institute of Child Health and Human Development, National Institutes of Health, Bethesda, MD, USA

[7] Tel Aviv University Sackler Faculty of Medicine, Maurice and Gabriela Goldschleger Eye Research Institute, Sheba Medical Center, Tel-Hashomer, Israel

[8] Hospital for Special Surgery, Weill Medical College of Cornell University, New York, NY, USA

Abstract

Osteogenesis imperfecta (OI) is most often caused by mutations in the type I procollagen genes (*COL1A1*/*COL1A2)*. We identified two children with substitutions in the type I procollagen C-propeptide cleavage site, which disrupt a unique processing step in collagen maturation and define a novel phenotype within OI. The patients have mild OI caused by mutations in *COL1A1* (Patient 1: p.Asp1219Asn) or *COL1A2* (Patient 2: p.Ala1119Thr), respectively. Patient 1 L1-L4 DXA z-score was +3.9 and pQCT vBMD was +3.1; Patient 2 had L1-L4 DXA z-score of 0.0 and pQCT vBMD of −1.8. Patient BMD contrasts with radiographic osteopenia and histomorphometry without osteosclerosis. Mutant procollagen processing is impaired in pericellular and *in vitro* assays. Patient dermal collagen fibrils have irregular borders. Incorporation of pC-collagen into matrix leads to increased bone mineralization. FT-IR imaging confirms elevated mineral/matrix ratios in both patients, along with increased collagen maturation in trabecular bone, compared to normal or OI controls. Bone mineralization density distribution revealed a marked shift toward increased mineralization density for both patients. Patient 1 has areas of higher and lower bone mineralization than controls; Patient 2's bone matrix has a mineral content exceeding even classical OI bone. These patients define a new phenotype of high BMD OI and demonstrate that procollagen C-propeptide cleavage is crucial to normal bone mineralization.

Corresponding Author: Joan C. Marini, MD, PhD, Chief, Bone and Extracellular Matrix Branch, NICHD, NIH ,Bldg. 10; Rm 10N260, 9000 Rockville Pike, Bethesda, MD 20892, (T)–301-594-3418, (F)–301-480-3188, oidoc@helix.nih.gov.
[§]These authors contributed equally to this manuscript

Keywords

Osteogenesis imperfecta; C-propeptide; collagen; C-proteinase; mineralization; high bone mass

Introduction

Autosomal dominant osteogenesis imperfecta (OI; MIM#s 166200, 166210, 259420, 166220) is caused by mutations within either of the type I procollagen genes, *COL1A1* (MIM# 120150) or *COL1A2* (MIM# 120160) (Marini, et al., 2007). Mild cases of OI are generally due to a *COL1A1* null allele, whereas moderate, progressively deforming, and perinatal lethal OI are caused by mutations that result in structural defects of one of the collagen α-chains. Affected individuals have bone fragility and low bone mass, often accompanied by short stature, blue sclerae, dentinogenesis imperfecta, and hearing loss (Marini, 2004), as well as increased mineralization density of bone matrix and impaired material properties (Boyde, et al., 1999; Roschger, et al., 2008b).

Type I collagen is a heterotrimer composed of two α1(I) and one α2(I) chains. The chains are synthesized as promolecules, with globular extensions at the amino (N-) and carboxyl (C-) ends. Chain selection and alignment occur in the C-propeptide region, followed by the folding of the triple helix from C- to N- end (Khoshnoodi, et al., 2006). The C-propeptide contains two intra- and four inter-chain disulfide bonds. After procollagen is secreted from the cell, it is processed by specific N- and C-proteinases in the pericellular space, releasing the mature collagen triple helical monomer. Normally, neither propeptide is incorporated into the higher order collagen fibril in the extracellular matrix.

The N-propeptide cleavage site consists of proα1(I) p.Pro161Gln162 and proα2(I) p.Ala79Gln80. Deficiency of N-propeptide cleavage results in a distinctive phenotype (Byers, et al., 1997; Cabral, et al., 2005). Impaired splicing of exon 6, which encodes the cleavage site, leads to retention of the N-propeptide and defective collagen cross-linking and results in Ehlers-Danlos Syndrome (EDS) VIIA (α1(I)) or B (α2(I)) (Byers, et al., 1997). In fact, some individuals with EDS VII also suffer fractures, as the retained N-propeptide may block mineral deposition (Byers, et al., 1997). In EDS VII, collagen fibrils have very irregular borders, high variability in diameter, and are more randomly spaced (Giunta, et al., 2008). A special subset of mutations in the first 90 residues of the α1(I) helical region prevent or delay N-propeptide removal by unfolding the cleavage site and lead to a combined OI/EDS phenotype (Cabral, et al., 2005). In OI/EDS patients, incorporation of the N-propeptide into matrix significantly reduces collagen fibril diameter (Cabral, et al., 2005). The OI component of OI/EDS has typical clinical findings of varying severity, including short stature and low bone density, intensely blue sclerae and early scoliosis.

Heterozygous mutations have been identified in the C-propeptide regions of both type I collagen alpha chains, with phenotypes ranging from mild to lethal OI; these rare mutations account for less than 5% of dominant OI (Chessler, et al., 1993; Pace, et al., 2008). Clinically, almost all of these individuals have typical OI with short stature and reduced bone mass. The intriguing exception is an atypical perinatal lethal case with radiographically dense bone, narrow marrow cavities and decreased osteoclasts associated with a heterozygous mutation (p.D1441Y) near the carboxyl end of the C-propeptide (Pace, et al., 2002). Although it is clear that these mutations delay chain incorporation into procollagen fibers (Chessler, et al., 1993; Pace, et al., 2008), the pathogenesis of their OI is not well understood. In the dense bone case, the authors speculated that increased mineralization or abnormal C-propeptide signaling might contribute to the phenotype.

Procollagen C-proteinase (PCP) activity for removal of the C-propeptide is provided by a number of tolloid-like proteinases, including bone morphogenic protein 1 (BMP1), which is the major PCP (Hopkins, et al., 2007; Kessler, et al., 1996; Li, et al., 1996), mammalian tolloid (mTld; an alternatively spliced form of BMP1) and two closely related homologs known as mammalian tolloid-like 1 and 2 (mTll1 and 2). In concert with enhancer proteins (PCPE1 and 2), PCP cleavage of the C-propeptides of types I-III procollagen by BMP1 is increased up to 10-fold (Kessler, et al., 1996; Moali, et al., 2005; Steiglitz, et al., 2002). The cleavage reaction occurs at the Ala-Asp (α1(I) p.Ala1218Asp1219; α2(I) p.Ala1119Asp1120) bonds that separate the C-telopeptide from the C-propeptide (Fig. 1). *Bmp1* knock-out mice are perinatal lethal (Suzuki, et al., 1996), as are *Bmp1*$^{-/-}$/*Tll1*$^{-/-}$ mice (Pappano, et al., 2003), in which redundancy for the BMP1 cleavage activity is eliminated. Of note, knock-out mice for *Pcolce*, which encodes PCPE1, survive and have a distinctive phenotype of massive bones yet with inferior material properties and altered mineral phase morphology by μCT (Steiglitz, et al., 2006).

We characterize here a novel form of OI, due to defects in the C-proteinase cleavage site. Two children, with mutations in either the proα1(I) or proα2(I) C-terminal cleavage site, have a distinctive OI phenotype in which bone fragility is associated with a counterintuitive increase of bone mass on DXA with respect to controls and/or other OI patients. Our investigations indicate that impaired type I collagen C-propeptide cleavage leads to increased bone matrix mineralization and modified collagen fibril structure.

Material and Methods

Mutation identification

COL1A1 (RefSeq NG_007400.1) and *COL1A2* (RefSeq NG_007405.1) of patient and parental leukocyte gDNA was sequenced as previously described (Matrix DNA Diagnostics, New Orleans, LA). For confirmation of the mutations, patient *COL1A1* (RefSeq NM_000088.3) and *COL1A2* (RefSeq NM_000089.3) cDNA was sequenced. The cDNA (c.) numbering is in accordance with journal guidelines (www.hgvs.org/mutnomen), with +1 corresponding to the first nucleotide of the ATG start codon and * representing sequence in the 3'UTR. Total RNA from patient fibroblasts was harvested with TriReagent (Molecular Research Center, Cincinnati, OH) and reverse-transcribed using a 3′ UTR anti-sense primer from *COL1A1* (c.*17-46, 5′-GGAAAGTTGGTTGGGTGGGAGGGAGCCAGG-3′) or *COL1A2* (c.*177-206, 5′-GGGGGAGCGGGGGAAGGAGTTAATGAAACT-3′). The region surrounding the C-propeptide cleavage site of both collagen chains was amplified by PCR (α1(I) exons 44 (c.3171-3200, 5′-TGGCCCTGCTGGCAAGAGTGGTGATCGTGG-3′) and 49 (c.3730-3759, 5′-CTTGCGGCTTCCCTCTGGGCTCCGGATGTT-3′) and α2(I) exons 48 (c.3195-3224, 5′–TGGTCGCACTGGACATCCTGGTACGGTTGG-3′) and 51 (c.3755-3784, 5′-TGGCCAGCAGGCGCATGAAGGCAAGTTGGG-3′)) and the RT-PCR products were sequenced using a CEQ2000 DNA Sequencer (Beckman, Fullerton, CA). Patient 2 and control gDNA was digested with *CviKI-1* for 4 hours at 37 °C and restriction fragments were resolved on a 10% polyacrylamide gel (PAGE).

Exons 2, 3, and 4 of the *LRP5* gene (RefSeq NM_002335.2) were amplified by PCR and sequenced for both patients, as previously described (Rickels, et al., 2005).

Collagen biochemical studies

For all collagen studies, control and patient fibroblasts were grown to confluence in 6-well culture dishes. Steady-state collagen analysis and pericellular processing were conducted as previously described (Cabral, et al., 2005). Cells were incubated with 437.5 μCi/ml of 3.96

TBq/mmol L-[2,3,4,5-^{3}H] proline for 16–18 hours or 24 hours for the steady-state and processing assays, respectively. The chain incorporation assay used the method of Chessler, et al (Chessler, et al., 1993). Briefly, procollagen alpha chains were labeled with a pulse of 140 μCi/ml of 3.96 TBq/mmol L-[2,3,4,5-^{3}H] proline for 80 minutes, then chased with DMEM containing 10% serum, 50 μg/ml ascorbic acid and 10 mM proline for the time intervals specified in the incorporation curve. Samples were ethanol precipitated and procollagens were separated by 5.5% SDS-Urea-PAGE. Differential scanning calorimetry (DSC) was performed in buffer containing 0.2 M sodium phosphate and 0.5M glycerol at pH 7.4, and analyzed from 10 to 55 °C in a Nano III DSC instrument (Calorimetry Sciences Corporation, Lindon, UT), as previously described (Makareeva, et al., 2008).

Preparation of ^{3}H-labelled Procollagen Substrate

To selectively label the C-propeptides, control and patient fibroblasts were grown to confluence in triple flasks (Nalge Nunc International, Rochester, NY) before labeling with ^{3}H-tryptophan. The day before labeling, cells were incubated with DMEM containing 10% serum, 50 μg/ml ascorbic acid, plus penicillin/streptomycin. Cells were labeled in serum-free DMEM containing 0.76 mg/L tryptophan, 75 μg/ml ascorbic acid and 2.4 μCi/mL ^{3}H-tryptophan overnight and media was collected with protease inhibitors. Radioactively labeled procollagen was precipitated in 6.25% Polyethylene glycol (PEG)4000. The pellets were dissolved in 0.1 M Tris-HCl, 0.4 M NaCl, pH 7.4. Insoluble material was removed by centrifugation and the supernatants were dialyzed against the Tris buffer. Radiolabeled fibronectin was removed by adsorption to Gelatin-Sepharose as described (Kessler, et al., 1986). Unbound procollagen samples were dialyzed against 0.1 M Tris-HCl, 0.4 M NaCl, pH 7.4. Procollagen concentrations were determined using the Sircol™ reagent (Biocolor, Carrickfergus, UK), with type I collagen as a standard. A procollagen:collagen ratio of 1.5:1 was used to calculated procollagen concentrations. The specific activities of the three procollagen preparations studied were 7.7 (control), 6.5 (Patient 1) and 7.2 (Patient 2) x10^6 cpm/mg, respectively. Procollagen was stored at −80 °C.

In vitro Assays of Procollagen C-proteinase Activity

To eliminate enhancing activity of endogenous PCPEs, procollagen samples were acidified (0.2 M acetic acid; 2 hrs at 4°C) and the pH was adjusted to 7.5 using 1 M Tris-HCl, pH 8.5, before conducting the assay. PCP activity was determined by measuring the amount of radioactively labeled C-propeptide released from control and patient procollagens, as described (Kessler, et al., 1986). Briefly, procollagen (15,000 cpm; 2 μg in 200 μl of 0.05 M Tris-HCl, 0.15 M NaCl, 5 mM $CaCl_2$) was incubated with BMP1 (37 ng) for either 60 min (control) or 120 min (patients). The reaction was stopped with EDTA and the free radioactive C-propeptide was separated from un/partially digested procollagen by selective ethanol precipitation (Kessler, et al., 1986). Radioactivity in the supernatants (containing the C-propeptide) was measured using a Packard Tri-carb 1600 CA β-counter. In another experiment, procollagen (8000 cpm, 1 μg) was incubated with BMP1 (5 ng) with or without PCPE1 (50 ng) for 120 mins in 40 μl of buffer. The reaction was stopped by heating in SDS sample buffer and electrophoresed on 5.5% SDS-Urea-PAGE. Radioactive proteins were visualized by autoradiography and relative band intensities were determined after scanning on optimized, non-edited images, using TINA image analysis software (ver.2.07d, Raytest isotopenmessgerete, GmBH), after background subtraction. Recombinant BMP1 and PCPE1 used in the *in vitro* assay were expressed in HEK-293 cells and purified as described (Moali, et al., 2005).

Transmission Electron Microscopy of Dermal Fibrils

Dermal punch biopsies from both patients and an age-matched control were fixed in 2.5% glutaraldehyde for 24 hours, then transferred to phosphate buffer. Fixed specimens were

treated with 1% osmium tetroxide, then 2% uranyl acetate, followed by infiltration by Spurr's plastic resin. Sections 600–800 Å in thickness were analyzed and photographed by transmission electron microscopy, as described (Cabral, et al., 2005).

Bone Histomorphometry

Both patients had iliac crest bone biopsies under anesthesia, following declomycin double labeling for kinetic analysis. Samples were fixed in 70% ethanol and embedded in polymethylmethacrylate (PMMA). Consecutive 3 μm thick sections were cut from the tissue block with a hard microtome (Leica SM2500, Nusslock, Germany). Sections were deplasticized with 2-methoxyethyl-acetate before staining with modified Goldner's Trichrome. Bone histomorphometric analysis was performed according to Parfitt, et al. (Parfitt, et al., 1987) on the whole area of the bone sections. A light microscope equipped with a Zeiss AxioCam videocamera was used to obtain digital images of the section which were analyzed used NIH Image software version 1.63 on a Power Macintosh G4.

Fourier transform infrared spectroscopy (FT-IR) analysis of bone

A portion of each iliac crest specimen was embedded in PMMA, sectioned at 2 μm, and mounted on barium fluoride spectral windows. FT-IR spectral images of three to five sections were recorded on a SpotLight 300 infrared imaging system (Perkin Elmer Instruments, Shelton, CT, USA). The spectral resolution was 4 cm^{-1}, and the pixel resolution was ~7 μm. Spectra were transferred to yield images corresponding to infrared band areas, peak height ratios and integrated area ratios by a combination of instrument software and ISYS chemical imaging software (v. 3.1, Spectral Dimensions Inc., Olney, MD, USA). Background spectra were collected under identical conditions from the same BaF_2 windows. After acquisition, spectra were truncated to allow analysis of the regions of interest, zero-corrected for baseline, and the spectral contribution of PMMA embedding media subtracted using ISYS software. Cortical and cancellous bone were examined separately in each section, and compared to 2 normal and 2 classical OI age-matched controls.

The parameters calculated for each image were i) mineral/matrix ratio (related to mineral content), calculated as the ratio of the integrated area under the phosphate band (920–1180 cm^{-1}) to that of the amide I band (1585–1720 cm^{-1}), and ii) carbonate-to-phosphate ratio (level of carbonate substitution in the hydroxyapatite crystal), calculated as the ratio of the integrated area of the carbonate peak (855–890 cm^{-1}) to the phosphate area. The crystallinity (related to crystallite size/perfection) was calculated from the intensity ratio of phosphate subbands at 1030 and 1020 cm^{-1}. The collagen maturity was calculated as the intensity ratio of amide I subbands at 1660 and 1690 cm^{-1}. Means and standard deviations for the three to five images in trabecular and cortical bone were calculated and compared. Heterogeneity of each image was calculated based on the full-width at half maximum of the pixel distribution.

Bone Mineralization Density Distribution (BMDD)

BMDDs were determined in the trabecular bone compartment of the transiliac biopsies using quantitative backscattered electron imaging (qBEI). Full details of the technique have been published (Roschger, et al., 1998; Roschger, et al., 2003). Blocks containing PMMA-embedded undecalcified iliac bone were prepared for qBEI by grinding and polishing to obtain plane parallel surfaces. qBEI makes use of the fact that the intensity of electrons backscattered from a depth of 1.5 microns from the surface-layer of a sectioned bone area is proportional to the weight concentration of calcium and thus mineral (hydroxyapatite) and calcium in bone. A digital electron microscope (DSM 962, Zeiss, Oberkochen, Germany) equipped with a four quadrant semiconductor backscattered electron BE detector was used.

The BE-signal (gray scale) was calibrated using the "atomic number contrast" between carbon (C, Z=6) and aluminum (Al, Z=13) as reference materials. Carbon was set to gray level index 25 and Al to 225, respectively. This allows a scaling also into weight % (wt%) Ca, whereby, osteoid (Z~6) has 0 wt% Ca and pure hydroxyapatite (Z=14.06) has 39.86 wt % Ca according to its composition. Thus, one gray level step corresponds to 0.17 wt% Ca after this calibration. Digital calibrated BE-images with a nominal 50x magnification (resolution 4 microns/pixel) were acquired, reflecting the spatial distribution of Ca-content. From these images, gray-level histograms (frequency distributions) were generated indicating the percentage of mineralized bone area (y axis) corresponding to the number of pixels with a certain gray level (x axis). The BE-image gray-level distribution can be interpreted as a wt% Ca bone mineralization density distribution (BMDD) for bone tissue or as mineralization density distribution for mineralized tissue in general.

Five parameters were deduced from the BMDD curve (Roschger, et al., 2008b): i) Ca_{Mean}, the weighted mean Ca concentration of the mineralized tissue area obtained from the integrated area under the BMDD curve; ii) Ca_{Peak}, the peak position of the histogram, which indicates the most frequently measured Ca concentration (Ca value with the highest number of pixels) in the measured bone area; iii) Ca_{Width}, the full width at half of the maximum distribution of the BMDD histogram curve describing the heterogeneity of mineralization caused by the co-existence of bone packets of different tissue age and therefore of different degrees of mineralization; iv) Ca_{Low}, the percentage of bone area that is mineralized below the fifth percentile in the reference range, i.e., below 17.68 wt% Ca (this parameter corresponds, therefore, also to the portion of bone area undergoing primary mineralization), and v) Ca_{High}, the percentage of bone area that is mineralized above the 95th percentile of the adult reference range (25.30 wt % Ca), and corresponds to the portion of highly mineralized bone matrix (Roschger, et al., 2008b).

Results

Clinical Descriptions of C-propeptide Cleavage Site Patients

Patient 1 (P1), a 13.5 yr old girl, was the 2950 g product of an uneventful pregnancy to a 39 yr old G5P3 Swedish woman. She was delivered vaginally at full term and had a normal newborn exam. Her developmental history was normal. At age 3.5 years, she incurred her first fractures (right tibia and fibula) after mild trauma. In subsequent years, the patient suffered 2–5 fractures/yr, including 3 upper extremity long bone, 3 olecranon, 4 tibial, 4 fibular and 4 small bone fractures of hands and feet. She has never been treated with an anti-resorptive drug. Clinical exam at age 12 years revealed white sclerae, normal dentition on inspection and radiographs, normal joint extensibility, straight spine and normal hearing and cardio-pulmonary evaluations. Bruising was slightly increased. Her growth and body habitus were normal, with height age of 161 cm at age 12 years (+1 SD compared to Swedish reference data), head circumference of 54 cm at 12 years (50^{th} percentile for age) and normal proportions (span:height ratio= 1.03; upper segment:lower segment ratio = 1.08).

Multiple evaluations of serum Ca, Mg, Vitamin D, phosphate and PTH were normal. L1-L4 DXA (Lunar Prodigy, GE Medical Systems) spine Z-scores at ages 8, 9.5, 11.5 and 12.5 years were +3.4, +2.8, +3.3, and +3.9; radial pQCT (XCT 2000, Stratec Medizintechnik GmbH, Pforzheim, Germany) at age 11.5 yielded a z-score = +3.1 total vBMD. Family members, including both parents, have lumbar spine DXA z-scores between +0.1 to +1.5, ruling out familial high bone mass. Despite Patient 1's elevated spine and wrist BMD, radiographic examination did not reveal signs of dense bone (Fig. 2). Long bones, especially fibulae, were not gracile, as would be common in OI. Radiographically, bone mass was diminished, appearing more osteopenic over time. Trabeculation was coarse throughout the skeleton, with persistence of larger trabeculae and loss of smaller trabeculae. There was a

loss of modeling in the distal ulna and radius; in the tibia/fibula there was periosteal reactive change. The lumbar and cervical vertebrae had a “bone-in-bone” appearance, despite no prior bisphosphonate therapy. The lumbar vertebrae were not expanded in a way that might artificially increase the BMD z-score. Mineralization of the skull appeared normal, with only a few wormian bones but without basilar invagination.

Patient 2 (P2), a 14 year old boy, is the offspring of non-consanguineous Caucasian American parents. He was the 3690 g product, delivered vaginally, of a full term pregnancy in a 32 year old G2P2 mother. Prenatal ultrasounds showed normal fetal development; post-natal development was normal. Starting at age 2 years, he sustained 8 long bone fractures in addition to several small bone fractures. At age 4.5 years, he was referred to a geneticist to rule out OI after osteopenia was noted during assessment of a metatarsal fracture. He has undergone three orthopaedic procedures, the first at age 5 years to stabilize an olecranon fracture with a pin, the second at age 10 for placement of intramedullary rods in the right femur, and the third at age 12 for placement of plate and screws on the distal left ulna.

On clinical exam at age 11.5 years, he had normal facies with light grey scleral hue, normal dentition, and unremarkable audiological and cardiovascular (ECHO/EKG) exams. He exhibited generalized joint hyperextensibility, with a Beighton score of 4/9 for bilateral elbows, the left knee and the ability to place the palms of has hands flat on the ground while bending down at the waist. His spine was straight. There was no bruising. Patient 2 had above average stature, with length that is 50% for a normal 12.5 year old boy, weight is 50% for an 11 year old and head circumference that is 50% for a 16 year old. There were no dysmorphic facial features. Dentinogenesis imperfecta was absent. Mild S-curve scoliosis has recently developed.

Serum Ca, Mg, Vitamin D, phosphate and PTH were normal. Patient 2 had received 6 cyles of bisphosphonate between ages 6–8 yr. His L1-L4 DXA (Hologic QDR 4500) z-score at age 12 years was average (0.00), while L1-L2 volumetric QCT (GE LightSpeed Ultra) z-score is −1.8. Radiographs of his lower extremity showed evidence of mild osteopenia (Fig. 2) but no evidence of dense bones. Lower limb long bones had dense metaphyseal transverse lines from cycled bisphosphonate, genu valgum, and tibial bowing. No vertebral compressions were seen, only mild concavity of lumbar vertebrae. Cervical spine CT showed no platybasia or basilar invagination.

Identification of C-propeptide Cleavage Site Mutations

The coding regions of the type I collagen genes, *COL1A1* and *COL1A2*, were completely sequenced. Patient 1 was found to have a heterozygous c.3655G>A substitution, causing an aspartic acid>asparagine change (p.Asp1219Asn) at the C-propeptide cleavage site in *COL1A1* (Figs. 1 and 3A). Her mutation was confirmed by cDNA sequencing. Sequencing of Patient 2 *COL1A1* and *COL1A2* genes (The Center for Gene Therapy, Tulane University) revealed a heterozygous c.3355G>A substitution causing an alanine>threonine change (p.Ala1119Thr) at the cleavage site of *COL1A2*. (Figs. 1 and 3B) We confirmed the mutation, which eliminated a *CviKI-I* restriction site, by amplification and digestion of patient gDNA. The collagen sequence changes were not found in either set of parents.

Mutations near the N-terminus of LDL-receptor related protein 5 (*LRP5*) cause both a benign high bone mass phenotype and high bone mass disease (Van Wesenbeeck, et al., 2003). Accordingly, we sequenced *LRP5* exons 2, 3 and 4, where all high bone mass mutations have been detected, but did not find any defects in our patients.

Collagen biochemistry is minimally altered

The steady-state fibroblast collagen from both children (Fig. 3C) had minimal electrophoretic abnormalities. Patient 1 had slightly delayed gel migration in the cell and media fractions, while Patient 2 collagen chains had normal mobility. Both patients had slight backstreaking of α1(I) and α2(I) cellular collagen, suggesting only a slight delay in the folding of the chains. Differential scanning calorimetry confirmed that collagen of both patients had normal thermal stability (Fig. 3D).

Incorporation of proα1(I) and proα2(I) chains into triple helices was measured (Fig. 3E), to determine whether C-propeptide cleavage site mutations delayed chain incorporation, as previously demonstrated for mutations in the C-propeptides (Chessler, et al., 1993). Patient 1 had normal chain incorporation, compared to control cells, while Patient 2 had a 20–40 minute delay in chain incorporation, suggesting the cleavage site substitution in proα2(I) may alter the structure of the chain recognition or alignment regions.

Procollagen pericellular and *in vitro* processing is delayed

Processing of the C-propeptide of patient procollagen was examined by pericellular and *in vitro* assays (Fig. 4). Patients 1 and 2 both had a substantial delay in pericellular procollagen processing compared to controls. (Fig. 4A) Patient 1 had a severe processing defect, with minimal cleavage of either α chain and accumulation of only a small amount of mature collagen in the media. Although Patient 2 appeared to be able to cleave α1(I) chains, only a minor amount of mature α2(I) chains was detected. In addition, increased amounts of uncleaved procollagen and pC-collagens (procollagen with N- but not C- end processed) were seen in both patients.

Pericellular procollagen processing assays reflect the combined activities of the various PCPs and their enhancer proteins, PCPE1 and 2. To examine the effect of the mutation on the activity of BMP1 and PCPE1 separately, *in vitro* quantitative assays were performed in which the ^{3}H-tryptophan labeled procollagen substrates were incubated with purified BMP1, with or without addition of PCPE1, and the amount of radioactivity in the released C-propeptide trimer was measured. The results of these assays revealed that the activity of BMP1 on Patient 1 and 2 procollagen was about 30% and 46% of control (data not shown), in good agreement with the 25 and 50% cleavage expected if the amino acid substitutions interfered with C-propeptide cleavage. Enhancing activity of PCPE1 was about half of normal toward Patient 1 procollagen, but comparable to control (≈ 4 fold) with Patient 2 procollagen. A marked reduction in C- terminal procollagen processing by BMP1 is also seen on the autoradiogram (Fig. 4B, right), with relatively lower amounts of free C1 and C2 in Patients 1 and 2, respectively, suggesting impaired cleavage of the mutant chains. Once again, enhancing activity of PCPE1 toward procollagen from Patient 1 but not from Patient 2, appeared to be reduced. Data obtained by densitometry revealed that processing of the mutant proα chain in both Patient 1 (α1(I)) and Patient 2 (α2(I)) was ~2 fold slower than that of the respective normal chains, seen with and without addition of PCPE1 (Table 1). This is also evident from the C1/C2 ratios: ~2:1, 1.5:1 and 4.9:1 for control, Patient 1 and Patient 2 procollagens, respectively (Table 1, Fig. 4B, right).

Incorporation of pC-collagen alters matrix fibrils

In *Bmp1*$^{-/-}$ and *Bmp1*$^{-/-}$/*Tll1*$^{-/-}$ mice, which cannot cleave the type I collagen C-propeptide because the processing enzyme is absent, incorporation of pC-collagen into fibrils results in a "barbed-wire" like appearance (Pappano, et al., 2003; Suzuki, et al., 1996). The dermal collagen fibrils of our patients have an irregular border on cross-section, compared to the smooth cross-sectional borders of fibrils from an age-matched control (Fig. 5). This is especially seen in Patient 2 fibrils, many of which have blebs protruding from the

surface. Fibril diameters were normal in Patient 1(88.3 ± 7.4), but with significantly increased variance compared to control (p=0.032). Patient 2 (71.2 ± 6.9) fibril diameters were significantly smaller than control (89.0 ± 6.4, p = <0.001) without higher diameter variability. The longitudinal views of patient collagen fibrils did not have an obvious "barbed-wire" appearance.

Histomorphometry of patient bone samples

Each patient underwent an iliac crest biopsy after declomycin labeling. The analyses of static and kinetic parameters revealed distinct patterns in each child, compared with those found in type I OI (Glorieux, et al., 2000) and in a reference population of 11–13.9 year old children (Table 2) (Rauch, et al., 2000).

Unlike type I OI patients, Patient 1 has normal ratio of bone volume to bone tissue, with increased trabecular number and reduced trabecular thickness. Osteoid seams, with and without osteoblasts, appeared several fold thicker than normal or type I OI, covering a greater portion of the trabecular surface and giving a picture of osteoidosis. (Fig. 6A) Osteoclast surface and number and eroded surface were increased. Mineral apposition (MAR) and bone formation (BFR/BS) rates were elevated compared to controls, suggesting that osteoblasts produced a greater amount of matrix which was incompletely mineralized.

For Patient 2, all structural indices were decreased compared to controls. However, bone volume/total volume (BV/TV) and trabecular number (Tb.N.) were increased compared to type I OI, while trabecular thickness (Tb.Th.) was normal. The osteoid thickness was within normal range, and thus markedly thinner than in Patient 1. Interestingly, most of the trabeculae appeared to be covered by thin osteoid seams without osteoblasts (Fig. 6B). In occasional areas, active osteoblasts and relatively thick osteoid were found. The osteoblast surface and eroded surface were normal in Patient 2. However, no active osteoclasts were seen in the sections. The portion of surface undergoing mineralization (MS/BS) was much smaller in Patient 2 than in Patient 1 and controls. MAR was elevated resulting in normal range BFR/BS, and indicating less brisk remodelling than in type I OI. Neither child had signs of osteosclerosis.

Increased mineralization of cortical and trabecular bone

To understand the unexpectedly normal or high BMD of our patients, we examined sections of their iliac crest bone by Fourier transform infrared (FT-IR) imaging. The mineral/ matrix ratio was significantly increased in both cortical and trabecular bone of Patient 1 and Patient 2, compared not only to two age-matched samples of control bone but also to bone from patients with classical OI caused by helical mutations in *COL1A2* (p.Gly280Val, α2(I)G190V; p.Gly1030Asp, α2(I)G940D)(Fig. 7A). The crystal size and perfection (crystallinity) of patient mineral was reduced in cortical bone, comparable to the crystallinity of classical OI cortical bone samples (Fig. 7B). The matrix phase of patient trabecular bone had a significant increase in collagen maturity compared to normal or classical OI bone (Fig. 7C), which may reflect increased proximity of cross-link sites due to altered folding of incorporated pC-collagen; the increase in maturity was not significant in patient cortical bone. The carbonate/phosphate ratio, a parameter indicative of carbonate substitution in the hydroxyapatite crystal, did not differ significantly among all OI or control samples (Fig. 7D). The heterogeneity of the mineral and crystallinity distribution was increased in the two patients for mineral/matrix ratio relative to both classic OI and the controls demonstrating the wide variation in mineral content across the sample in both cortical and trabecular regions. The greatest spread in the data was seen in the mineral/matrix ratio and collagen maturity in Patient 1. This distribution can be seen in the representative images for Patient 1 and classic OI (Fig. 7A-D).

Patient BMDDs show increased matrix mineralization

The BMDDs of the patients were measured using quantitative backscattered electron imaging (qBEI). Both patients exhibited BMDDs with a significant shift towards increased matrix mineralization compared to a young reference cohort (Fratzl-Zelman, et al., 2009) but their mineralization patterns were different. For Patient 1**,** the BMDD peak was remarkably broadened although the peak was shifted to a lesser extent than for Patient 2 (Fig. 8C). Patient 1 had matrix areas of both higher (black arrow) and lower mineral content (white arrows) (Fig. 8A), while Patient 2 had a more uniformly higher mineral content throughout the bone sample (Fig. 8B).

The patient BMDDs were compared to two classical OI bone samples and to a previously published cohort of type I OI cases (Fratzl-Zelman, et al., 2010) (Fig. 8C and Table 3). Patient 1 had increased Ca_{Mean}, Ca_{Peak}, and Ca_{High}, similar to classical OI bone, in which increased mineral content compared to normal pediatric bone was previously demonstrated (Roschger, et al., 2008a; Weber, et al., 2006). However, Patient 1 also had a distinctive increase in Ca_{Width}, reflecting an increase in heterogeneity of mineralization. Patient 2 had a higher Ca_{Mean} than all other OI and control samples, demonstrating uniformly high bone mineralization. Furthermore, the bone area undergoing primary mineralization (Ca_{Low}) was approximately doubled in Patient 1 compared to control and OI samples, while the portion of highly mineralized areas (Ca_{High}) in Patient 2 was increased 50-fold compared to control and about 3-fold compared to classical OI bone. These findings have not been noted in other OI children before or after bisphosphonate treatment (Weber, et al., 2006).

Discussion

We report here the first studies of patients with collagen mutations causing defective processing at the type I procollagen C-propeptide cleavage site. The two affected children have substitutions which block removal of the C-propeptide and cause OI with a distinctive high bone mass phenotype. The patients have elevated DXA measurements with respect to controls and/or other OI patients, which is caused by increased bone mineralization. FT-IR and BMDD demonstrate that these patients have elevated mineral/bone matrix, compared to OI cases with structural defects in the collagen helix and age-matched controls. The pamidronate infusions received by Patient 2 had been completed 4 years before our studies and would not have affected the distinctive bone findings. Specifically, although bisphosphonate increases the mineral/matrix ratio detected by FT-IR (Gourion-Arsiquaud, et al., 2010), Patient 2's normal growth rate in the years since treatment would have replaced most of the iliac bone (Glorieux, et al., 2000) with his baseline bone composition. In addition, BMDD results have been shown to be unchanged by bisphosphonate treatment (Weber, et al., 2006).

Clinically our patients have mild phenotypes with normal growth, white or light grey sclerae, straight spines and normal dentition, hearing and cardiopulmonary exams. Their type I collagen has minimal biochemical abnormality. Pericellular processing, however, is significantly delayed, especially for procollagen with a proα1(I) p.Asp1219Asn substitution, from which only a small amount of mature collagen was detected. The minimal cleavage of either the proα1(I) or proα2(I) chain in Patient 1 was consistent with studies using purified C-proteinase which showed that both proα1(I) chains were cleaved from the heterotrimer before proα2(I) cleavage occurs (Njieha, et al., 1982). The proα2(I) p.Ala1119Thr substitution allows the majority of α1(I) chains to be cleaved, but interferes with proα2(I) processing. *In vitro* processing of our patients' procollagen with purified BMP1 supports the interpretation that the C-propeptide trimer can be processed normally only if the cleavage site is intact in all three chains. PCPE1 activity depends on its binding to the procollagen C-propeptide (Kessler, et al., 1996). Although PCPE1 bound normally to Patient 1 procollagen

(data not shown), its enhancing activity toward cleavage was about half of control. The marked reduction in pericellular processing of Patient 1 procollagen may reflect the combined effect of the patient's mutation on both BMP1 and PCPE1 activity.

Several other individuals with mutations affecting the C-propeptide cleavage site have been identified, but their collagen biochemistry and bone mineralization have not been studied (Fig. 1). High bone mass is a consistent finding in these individuals. At the same Asp residue in the proα1(I) cleavage site (p.Asp1219) at which our Patient 1 has an Asn substitution, a Glu substitution was associated with "type I OI" in several generations (Pollitt, et al., 2006). Affected individuals had fractures, normal teeth and normal hearing. A Thr substitution at the Ala residue in the proα1(I) cleavage site (p.Ala1218) was reported in two adult siblings with scoliosis, who had incurred dozens of long bone fractures (Cundy, et al., 2008). These adults had elevated DXA BMD z-scores, as well as normal stature, white sclerae, and normal dentition. Unlike our pediatric patients, they have a significant conductive hearing loss. A defect in the remaining cleavage site residue, proα2(I) p.Asp1120, was recently identified in a large Iraqi pedigree with DXA z-scores elevated up to +3.5 SD, severe joint laxity and blue sclerae (Li, 2009).

Histomorphometry of our patients' bone revealed near normal trabecular bone volume, although their bone appeared osteopenic on radiographs. Trabecular thickness but not trabecular number was reduced. The bone of Patient 1 had thick osteoid seams, as was also found with the α1(I) p.Ala1218Thr substitution (Cundy, et al., 2008), suggesting this finding may be related to failure to cleave proα1(I). The majority of proα1(I) C-propeptides are cleaved in Patient 2, and he had only occasional areas with thick osteoid seams. Neither child had signs of osteosclerosis as reported for the adults with the proα1(I) p.Ala1218 substitution. Accordingly, we propose that osteosclerosis may develop with age, as turnover of abnormal bone becomes more difficult.

Patients with defects in the C-propeptide cleavage site can be compared to murine defects in the C-proteinase and its enhancer protein. Homozygous knock-out mutations in procollagen C-proteinase alone (*Bmp1*$^{-/-}$ mice) (Suzuki, et al., 1996), or in combination with a null mutation in Tolloid-like protein 1 (*Bmp1*$^{-/-}$/*Tll1*$^{-/-}$) to eliminate redundant cleavage activity (Pappano, et al., 2003), are perinatal lethal and result in thin collagen fibrils with a "barbed-wire" appearance. The barbs were hypothesized to be retained C-propeptide on the fibril surface, and C-propeptide retention was demonstrated by immunofluorescence (Steiglitz, et al., 2006). In contrast, fibrils in our patients have a normal longitudinal appearance, but are abnormal on cross-section. Blebs (Fig. 5) are detected on the surface of many fibrils, especially in Patient 2. We speculate that more blebs are seen in Patient 2 than Patient 1 because retained C-propeptide in Patient 1 may be in a configuration that favors non-specific cleavage. Fibril diameters in Patient 1 are normal, whereas those of Patient 2 are small. The patient fibrils resemble those from mice with null mutations in the procollagen C-proteinase enhancer (*Pcolce*$^{-/-}$), which have irregular scalloped borders on cross-section. These mice survive and have massive bones with excess bone deposition and increased trabecular number, but inferior material properties (Steiglitz, et al., 2006) which the authors hypothesized might be due to abnormal interactions of collagen matrix and mineral. The greater severity of *Pcolce*$^{-/-}$ bone and fibril findings compared to our patients is likely to be related to diminished cleavage of multiple fibrillar procollagens in the absence of the enhancer protein, including types I, II, III and V procollagen (Moali, et al., 2005; Steiglitz, et al., 2006), versus partial failure to cleave type I procollagen in our patients.

Retention of the type I procollagen C-propeptide in our two patients has the distinctive effect of increasing bone mineralization, although with a different distribution in each child. While Patient 1 shows a broadened BMDD peak, indicating increased heterogeneity of

mineralization and bone packets of different ages, Patient 2's narrow peak indicates more homogenous mineralization. Patient 2's peak is shifted to an even higher average mineralization than found in children with classical OI. Both bone remodeling and mineralization kinetics of newly deposited bone are reflected in BMDD. Therefore, the distinct broadening of the BMDD peak in Patient 1 suggests a high number of active sites for new bone formation, resulting in incompletely mineralized matrix, as seen in the BEI images and consistent with the thick osteoid seams on trabecular surfaces, and the elevated BFR/BS and MAR found on histomorphometry. Patient 2 has a lower number of active bone formation sites than Patient 1. However, the thin osteoid seams covering 80% of trabecular surfaces, the marked increase in MAR and reduced resorptive activity suggest that his osteoblasts synthesize larger amounts of matrix than do control or classical OI children and that the bone packets have time for secondary mineralization.

Furthermore, since the bone matrix in both children can be mineralized more highly than in controls, their mineralization process is profoundly altered. Given the location of the C-terminal end of type I collagen on the surface of the heterotypic collagen fibril (Orgel, et al., 2006; Orgel, et al., 2000; Perumal, et al., 2008), we hypothesize that their C-propeptides are retained on the fibril surface long enough to affect the mineralization process. They may do this by increasing the intra-fibrillar spacing, or by directly serving as nucleators of mineralization. Both the excess mineral *per se* and the discontinuities in the bone material may increase bone fragility.

Acknowledgments

We would like to thank Drs. Art Veis and Joseph Orgel for thoughtful discussion of preliminary data; Gerda Dinst, Phaedra Messmer and Daniela Gabriel for careful bone sample preparations and qBEI measurements; Prof. Jan Gustafsson, MD, PhD and Jan Engvall, MD, for initial clinical assessment and referral of Patient 1; Catherine Reisenberg, FNP, Ph.D., for assembly of clinical data on Patient 2; Ivan Budnik, MD, for help with the densitometry experiments, and Anna-Lena Johansson for skillful technical assistance. A special thanks to the patients and their families for dedication to this study.

This work was supported by NICHD Intramural Funding (JCL and SL); grants from the Swedish research council (#207-2946) (KL and OL); grant 1360/07 from the Israel Science Foundation (EK); NIH grants DE04141 and AR041325 (ALB), AUVA (Research funds of the Austrian workers compensation board) and WGKK (Viennese sickness insurance funds) (NF-Z, PR and KK).

References

Boyde A, Travers R, Glorieux FH, Jones SJ. The mineralization density of iliac crest bone from children with osteogenesis imperfecta. Calcif Tissue Int. 1999; 64(3):185–90. [PubMed: 10024373]

Byers PH, Duvic M, Atkinson M, Robinow M, Smith LT, Krane SM, Greally MT, Ludman M, Matalon R, Pauker S, et al. Ehlers-Danlos syndrome type VIIA and VIIB result from splice-junction mutations or genomic deletions that involve exon 6 in the COL1A1 and COL1A2 genes of type I collagen. Am J Med Genet. 1997; 72(1):94–105. [PubMed: 9295084]

Cabral WA, Makareeva E, Colige A, Letocha AD, Ty JM, Yeowell HN, Pals G, Leikin S, Marini JC. Mutations near amino end of alpha1(I) collagen cause combined osteogenesis imperfecta/Ehlers-Danlos syndrome by interference with N-propeptide processing. J Biol Chem. 2005; 280(19): 19259–69. [PubMed: 15728585]

Chessler SD, Wallis GA, Byers PH. Mutations in the carboxyl-terminal propeptide of the pro alpha 1(I) chain of type I collagen result in defective chain association and produce lethal osteogenesis imperfecta. J Biol Chem. 1993; 268(24):18218–25. [PubMed: 8349697]

Cundy, T.; King, A.; Byers, PH. Calcified Tissue International. 2008. A Novel Disorder of Type I Collagen Characterised by High Bone Mass, a Mineralization Defect and Tendon Calcification; p. 82S1

Fratzl-Zelman N, Morello R, Lee B, Rauch F, Glorieux FH, Misof BM, Klaushofer K, Roschger P. CRTAP deficiency leads to abnormally high bone matrix mineralization in a murine model and in children with osteogenesis imperfecta type VII. Bone. 2010; 46(3):820–6. [PubMed: 19895918]

Fratzl-Zelman N, Roschger P, Misof BM, Pfeffer S, Glorieux FH, Klaushofer K, Rauch F. Normative data on mineralization density distribution in iliac bone biopsies of children, adolescents and young adults. Bone. 2009; 44(6):1043–8. [PubMed: 19268565]

Giunta C, Chambaz C, Pedemonte M, Scapolan S, Steinmann B. The arthrochalasia type of Ehlers-Danlos syndrome (EDS VIIA and VIIB): the diagnostic value of collagen fibril ultrastructure. Am J Med Genet A. 2008; 146A(10):1341–6. [PubMed: 18409203]

Glorieux FH, Travers R, Taylor A, Bowen JR, Rauch F, Norman M, Parfitt AM. Normative data for iliac bone histomorphometry in growing children. Bone. 2000; 26(2):103–9. [PubMed: 10678403]

Gourion-Arsiquaud S, Allen MR, Burr DB, Vashishth D, Tang SY, Boskey AL. Bisphosphonate treatment modifies canine bone mineral and matrix properties and their heterogeneity. Bone. 2010; 46(3):666–72. [PubMed: 19925895]

Hopkins DR, Keles S, Greenspan DS. The bone morphogenetic protein 1/Tolloid-like metalloproteinases. Matrix Biol. 2007; 26(7):508–23. [PubMed: 17560775]

Kessler E, Adar R, Goldberg B, Niece R. Partial purification and characterization of a procollagen C-proteinase from the culture medium of mouse fibroblasts. Coll Relat Res. 1986; 6(3):249–66. [PubMed: 3533405]

Kessler E, Takahara K, Biniaminov L, Brusel M, Greenspan DS. Bone morphogenetic protein-1: the type I procollagen C-proteinase. Science. 1996; 271(5247):360–2. [PubMed: 8553073]

Khoshnoodi J, Cartailler JP, Alvares K, Veis A, Hudson BG. Molecular recognition in the assembly of collagens: terminal noncollagenous domains are key recognition modules in the formation of triple helical protomers. J Biol Chem. 2006; 281(50):38117–21. [PubMed: 17082192]

Li, C. Increased Bone Mineral Density and Body Mass Index in Families of Osteogenesis Imperfecta: a New Type of OI?. Honolulu, HI: 2009.

Li SW, Sieron AL, Fertala A, Hojima Y, Arnold WV, Prockop DJ. The C-proteinase that processes procollagens to fibrillar collagens is identical to the protein previously identified as bone morphogenic protein-1. Proc Natl Acad Sci U S A. 1996; 93(10):5127–30. [PubMed: 8643539]

Makareeva E, Mertz EL, Kuznetsova NV, Sutter MB, DeRidder AM, Cabral WA, Barnes AM, McBride DJ, Marini JC, Leikin S. Structural heterogeneity of type I collagen triple helix and its role in osteogenesis imperfecta. J Biol Chem. 2008; 283(8):4787–98. [PubMed: 18073209]

Marini, JC. Osteogenesis imperfecta. In: Behrman, RE.; Kliegman, RM.; Jensen, HB., editors. Nelson Textbook of Pediatrics. Philadelphia: W.B. Saunders; 2004. p. 2336-2338.

Marini JC, Forlino A, Cabral WA, Barnes AM, San Antonio JD, Milgrom S, Hyland JC, Korkko J, Prockop DJ, De Paepe A, et al. Consortium for osteogenesis imperfecta mutations in the helical domain of type I collagen: regions rich in lethal mutations align with collagen binding sites for integrins and proteoglycans. Hum Mutat. 2007; 28(3):209–21. [PubMed: 17078022]

Moali C, Font B, Ruggiero F, Eichenberger D, Rousselle P, Francois V, Oldberg A, Bruckner-Tuderman L, Hulmes DJ. Substrate-specific modulation of a multisubstrate proteinase. C-terminal processing of fibrillar procollagens is the only BMP-1-dependent activity to be enhanced by PCPE-1. J Biol Chem. 2005; 280(25):24188–94. [PubMed: 15834133]

Njieha FK, Morikawa T, Tuderman L, Prockop DJ. Partial purification of a procollagen C-proteinase. Inhibition by synthetic peptides and sequential cleavage of type I procollagen. Biochemistry. 1982; 21(4):757–64. [PubMed: 7041964]

Orgel JP, Irving TC, Miller A, Wess TJ. Microfibrillar structure of type I collagen in situ. Proc Natl Acad Sci U S A. 2006; 103(24):9001–5. [PubMed: 16751282]

Orgel JP, Wess TJ, Miller A. The in situ conformation and axial location of the intermolecular cross-linked non-helical telopeptides of type I collagen. Structure. 2000; 8(2):137–42. [PubMed: 10673433]

Pace JM, Chitayat D, Atkinson M, Wilcox WR, Schwarze U, Byers PH. A single amino acid substitution (D1441Y) in the carboxyl-terminal propeptide of the proalpha1(I) chain of type I collagen results in a lethal variant of osteogenesis imperfecta with features of dense bone diseases. J Med Genet. 2002; 39(1):23–9. [PubMed: 11826020]

Pace JM, Wiese M, Drenguis AS, Kuznetsova N, Leikin S, Schwarze U, Chen D, Mooney SH, Unger S, Byers PH. Defective C-propeptides of the proalpha2(I) chain of type I procollagen impede molecular assembly and result in osteogenesis imperfecta. J Biol Chem. 2008; 283(23):16061–7. [PubMed: 18375391]

Pappano WN, Steiglitz BM, Scott IC, Keene DR, Greenspan DS. Use of Bmp1/Tll1 doubly homozygous null mice and proteomics to identify and validate in vivo substrates of bone morphogenetic protein 1/tolloid-like metalloproteinases. Mol Cell Biol. 2003; 23(13):4428–38. [PubMed: 12808086]

Parfitt AM, Drezner MK, Glorieux FH, Kanis JA, Malluche H, Meunier PJ, Ott SM, Recker RR. Bone histomorphometry: standardization of nomenclature, symbols, and units. Report of the ASBMR Histomorphometry Nomenclature Committee. J Bone Miner Res. 1987; 2(6):595–610. [PubMed: 3455637]

Perumal S, Antipova O, Orgel JP. Collagen fibril architecture, domain organization, and triple-helical conformation govern its proteolysis. Proc Natl Acad Sci U S A. 2008; 105(8):2824–9. [PubMed: 18287018]

Pollitt R, McMahon R, Nunn J, Bamford R, Afifi A, Bishop N, Dalton A. Mutation analysis of COL1A1 and COL1A2 in patients diagnosed with osteogenesis imperfecta type I-IV. Hum Mutat. 2006; 27(7):716. [PubMed: 16786509]

Rauch F, Travers R, Parfitt AM, Glorieux FH. Static and dynamic bone histomorphometry in children with osteogenesis imperfecta. Bone. 2000; 26(6):581–9. [PubMed: 10831929]

Rickels MR, Zhang X, Mumm S, Whyte MP. Oropharyngeal skeletal disease accompanying high bone mass and novel LRP5 mutation. J Bone Miner Res. 2005; 20(5):878–85. [PubMed: 15824861]

Roschger P, Fratzl-Zelman N, Misof BM, Glorieux FH, Klaushofer K, Rauch F. Evidence that abnormal high bone mineralization in growing children with osteogenesis imperfecta is not associated with specific collagen mutations. Calcif Tissue Int. 2008a; 82(4):263–70. [PubMed: 18311573]

Roschger P, Fratzl P, Eschberger J, Klaushofer K. Validation of quantitative backscattered electron imaging for the measurement of mineral density distribution in human bone biopsies. Bone. 1998; 23(4):319–26. [PubMed: 9763143]

Roschger P, Gupta HS, Berzlanovich A, Ittner G, Dempster DW, Fratzl P, Cosman F, Parisien M, Lindsay R, Nieves JW, et al. Constant mineralization density distribution in cancellous human bone. Bone. 2003; 32(3):316–23. [PubMed: 12667560]

Roschger P, Paschalis EP, Fratzl P, Klaushofer K. Bone mineralization density distribution in health and disease. Bone. 2008b; 42(3):456–66. [PubMed: 18096457]

Steiglitz BM, Keene DR, Greenspan DS. PCOLCE2 encodes a functional procollagen C-proteinase enhancer (PCPE2) that is a collagen-binding protein differing in distribution of expression and post-translational modification from the previously described PCPE1. J Biol Chem. 2002; 277(51): 49820–30. [PubMed: 12393877]

Steiglitz BM, Kreider JM, Frankenburg EP, Pappano WN, Hoffman GG, Meganck JA, Liang X, Hook M, Birk DE, Goldstein SA, et al. Procollagen C proteinase enhancer 1 genes are important determinants of the mechanical properties and geometry of bone and the ultrastructure of connective tissues. Mol Cell Biol. 2006; 26(1):238–49. [PubMed: 16354695]

Suzuki N, Labosky PA, Furuta Y, Hargett L, Dunn R, Fogo AB, Takahara K, Peters DM, Greenspan DS, Hogan BL. Failure of ventral body wall closure in mouse embryos lacking a procollagen C-proteinase encoded by Bmp1, a mammalian gene related to Drosophila tolloid. Development. 1996; 122(11):3587–95. [PubMed: 8951074]

Van Wesenbeeck L, Cleiren E, Gram J, Beals RK, Benichou O, Scopelliti D, Key L, Renton T, Bartels C, Gong Y, et al. Six novel missense mutations in the LDL receptor-related protein 5 (LRP5) gene in different conditions with an increased bone density. Am J Hum Genet. 2003; 72(3):763–71. [PubMed: 12579474]

Weber M, Roschger P, Fratzl-Zelman N, Schoberl T, Rauch F, Glorieux FH, Fratzl P, Klaushofer K. Pamidronate does not adversely affect bone intrinsic material properties in children with osteogenesis imperfecta. Bone. 2006; 39(3):616–22. [PubMed: 16644299]

Figure 1.

Schematic diagram showing mutations identified at the four conserved C-propeptide cleavage site residues of *COL1A1* and *COL1A2*. [a](Cundy, et al., 2008), [b](Pollitt, et al., 2006), [c](Li, 2009)

Figure 2.

Patient radiographs show a generalized decrease in bone mass. The skull radiograph of Patient 1 shows few wormian bones, while her vertebral bodies have *os en os* without compressions. Patient 2 also has *os en os* vertebral bodies, perhaps a reflection of prior bisphosphonate therapy, but without compressions. The lower extremities show genu valgum, gracile midshafts of the femora, dense traverse lines from cycled bisphosphonate therapy, tibial bowing and a healed left fibular fracture. His thorax is long and narrow.

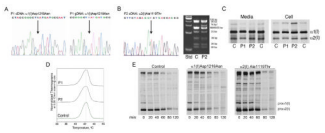

Figure 3.

Sequence and biochemistry of type I collagen. (**A**) Sequence tracings of Patient 1 cDNA and gDNA show the heterozygous G>A change in the α1(I) cleavage site. (**B**) The sequence tracing of Patient 2 cDNA shows the heterozygous G>A mutation in the α2(I) C-propeptide cleavage site (left) and a *CviKI-I* restriction enzyme digest of Patient 2 gDNA confirms the presence of the mutation (right). (**C**) The steady-state type I collagen protein from Patient 1 and Patient 2 dermal fibroblasts has slight backstreaking of the α1(I) and α2(I) chains in the cell fraction. (**D**) Differential scanning calorimetry reveals that the secreted procollagen of both patients has normal thermal stability. (**E**) A chain incorporation assay demonstrates that Patient 1 procollagen was incorporated normally into heterotrimers, while the incorporation of Patient 2 procollagen was only slightly delayed.

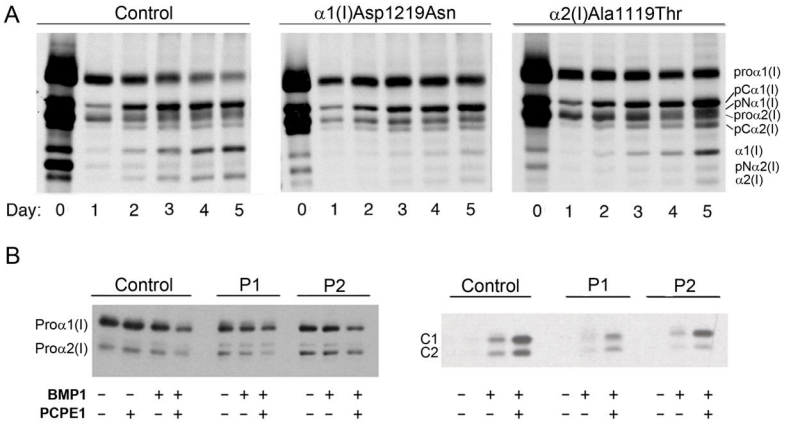

Figure 4.

Procollagen with a cleavage site mutation has delayed C-propeptide processing. **(A)** Pericellular processing of type I collagen from Patient 1 shows delayed processing kinetics, increased pro-α1(I) and pCα1(I) and much less mature collagen formation than control. Patient 2 has slightly delayed processing kinetics, increased pro-α1(I), pCα1(I), and slightly increased pro-α2(I) and pCα2(I) forms with less mature α2(I) collagen formed than in control fibroblasts. (**B**) Autoradiograms show that processing of the mutated pro-α chains from Patient 1 and Patient 2 by BMP1 is markedly reduced (left panel). The enhancing activity of PCPE1 is reduced only toward Patient 1 procollagen. Processing of the mutant proα chain (pro-α1(I) in Patient 1 and pro-α2(I) in Patient 2) appears to be preferentially affected, as evident in the right panel, showing the C-propeptide subunit bands, C1 and C2.

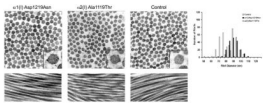

Figure 5.
Fibrils with a cleavage site mutation have irregular cross-sections and normal or decreased diameter. Dermal collagen fibrils from skin punch biopsies were examined by transmission electron microscopy. The fibril diameter was measured (n = 200) and compared with an age-appropriate control. Both Patient 1 and Patient 2 have irregular cross-sections with some blebs, while Patient 1 fibrils were normal in diameter and Patient 2 fibrils were decreased in size. Longitudinal cross-sections were normal with no appearance of branching or barbs.

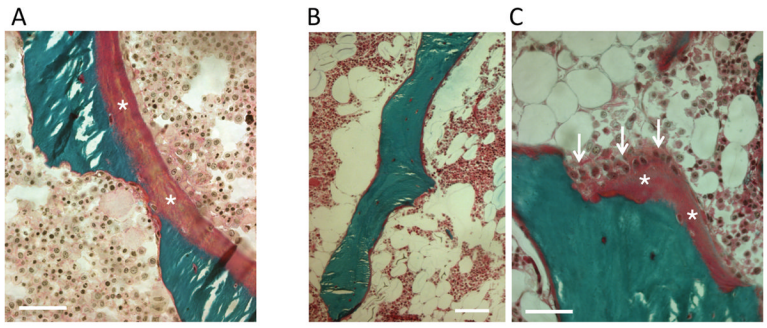

Figure 6

. Patients have abnormal osteoid formation. Light microscopic analysis of transiliac bone sections. Goldner's trichrome staining represents mineralized bone matrix in green and osteoid in purple. (**A**) Patient 1 has thick osteoid seams in purple (asterix) on the mineralized bone surface (bar represents 50 μm). (**B**) Patient 2 has generally thin osteoid, covering the mineralized (green) trabecular surface (bar represents 100 μm). (**C**) Patient 2: a focal area at higher magnification showing a thicker osteoid (asterix) with active osteoblasts (arrows) (bar represents 50 μm).

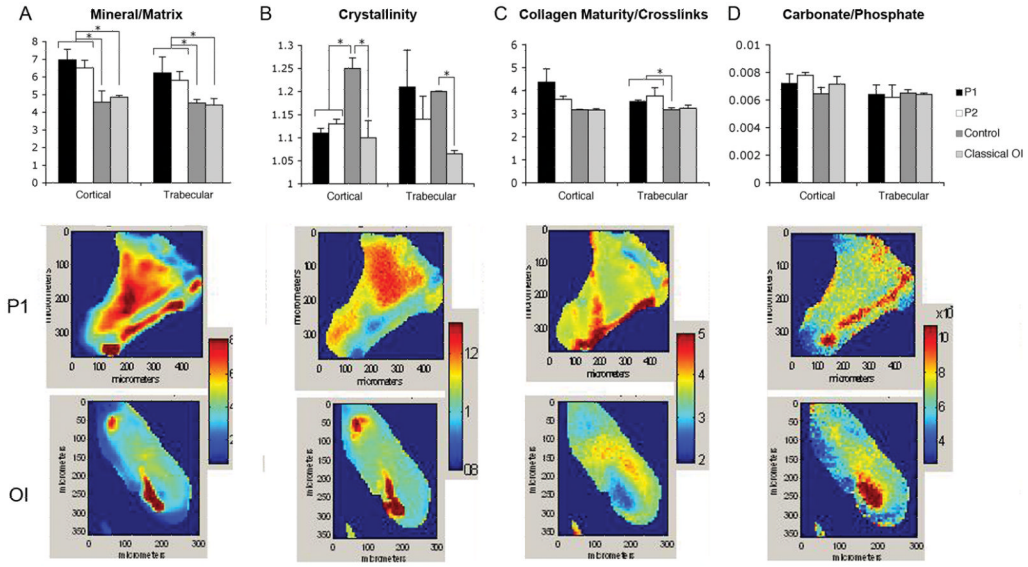

Figure 7.

Composition of iliac crest bone from patients with the C-propeptide cleavage site mutation, classical OI, and age-matched controls as determined by Fourier-Transform Infrared Imaging (FT-IR) Spectroscopy. The four parameters listed in the top row were measured for all cases and mean +/− SD for 3 areas of cortical and 3 areas of trabecular bone are shown, with * representing significant differences relative to the bracketed group, $p<0.05$ based on a t-test. Typical images from P1 and from a classic OI case are shown for each parameter. (**A**) Both C-propeptide mutation patients had an elevated mineral to matrix ratio in cortical and trabecular bone, compared to both two normal control and two classical OI samples. The mineral to matrix ratio as determined by FT-IR is directly related to the mineral content of the tissue. (**B**) Cortical crystallinity, a parameter related to the crystal size and perfection in the c-axis direction of the apatite crystals, was significantly decreased in the patients relative to controls and comparable to classic OI samples. (**C**) Cleavage site patients had an increase of trabecular collagen cross-links and a trend toward increased cortical cross-links. The collagen cross-link ratio is an indication of the maturity of the collagen, and does not provide information on the nature of the cross-links. (**D**) Carbonate to phosphate ratio (mineral composition), which indicates the extent of carbonate substitution in the apatites, did not vary significantly among samples.

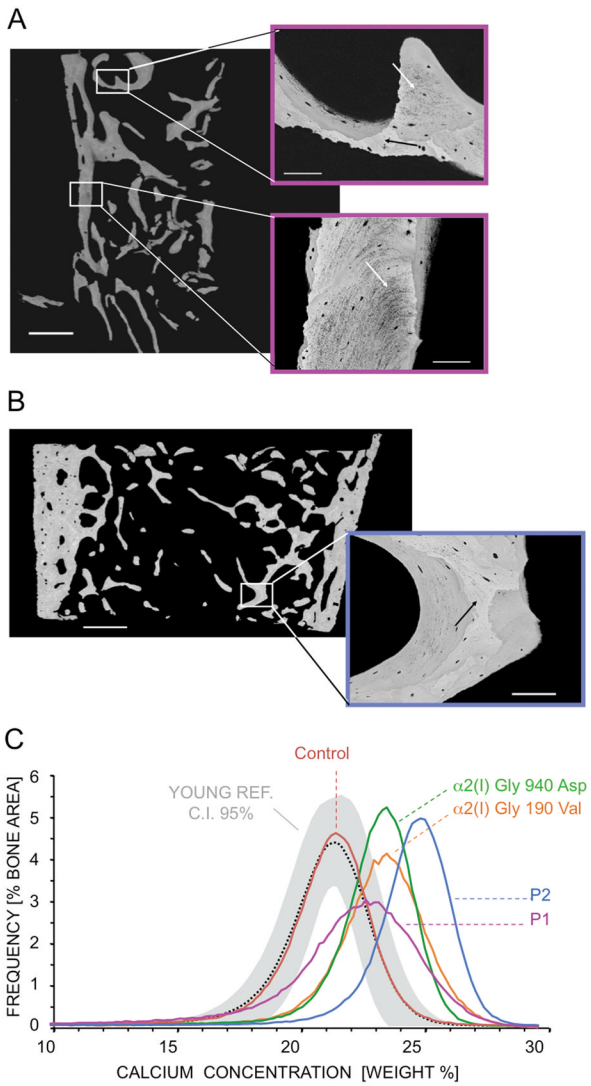

Figure 8.

Mineral content and organization of patient bone is altered. **(A)** Backscattered electron imaging (BEI) of Patient 1 bone samples demonstrates abnormal structure of mineralized bone matrix, both areas of higher (black arrow) and lower (white arrows) mineral content (see insets). (**B**) BEI of Patient 2 bone samples reveal a more homogenous and higher mineralized bone matrix. Black arrow (see inset) indicates an interstitial bone area of extremely high mineral content. (**C**) Bone mineralization density distribution (BMDD) demonstrates that for both patients BMDD is shifted towards higher mineral content compared to 54 normal pediatric bone samples from Young's reference. While Patient 1 shows a strong broadening of the BMDD peak width, Patient 2 shows a narrow peak width and the BMDD peak position shows a distinctly higher mineralization than even that of classical OI. The single control sample and the two classical OI samples showed similar results compared to the previously published controls (Fratzl-Zelman et al., 2009) and classical OI sample data (Roschger, et al., 2008a; Roschger, et al., 2008b; Weber, et al., 2006). Scale bar: overview - 1 mm; insets - 100 μm.

Table 1

Procollagen Processing

	Control	P1	P2
		(% Processed)	
BMP1 alone			
Proα1	14.4 ± 1.4	13.3 ± 0.3	11.7 ± 1.5
Proα2	17.8 ± 1.0	28.5 ± 2.1	4.5 ± 0.7
Proα2/Proα1	1.24	2.2	0.4
BMP1+PCPE1			
Proα1	55.0 ± 7.0	31.0 ± 1.0	53.7 ± 4.0
Proα2	60.0 ± 2.8	68.0 ± 1.4	29.4 ± 1.2
Proα2/Proα1	1.1	2.2	0.55
PCPE1 Fold Enhancement			
Proα1	3.8 ± 0.1	2.1 ± 0.3	4.5 ± 0.7
Proα2	3.4 ± 0.3	1.8 ± 0.1	5.3 ± 0.4
C1/C2 ratio*	1.9	1.5	4.9

Values represent mean ± SD (n=2–3)

* based on results obtained in the presence of PCPE1 shown in the right panel of Fig. 4B.

Table 2

Bone Histomorphometric Parameters

Bone Histomorphometric parameters	Reference Children 11–13.9 yrs*	P1	P1 vs. controls	P1 vs. OI	P2	P2 vs. controls	P2 vs. OI	OI Type I**
BV/TV	24.4 ± 4.2	27.83	0.82	3.24	19.87	−1.08	1.70	11.0 ± 5.2
mdBV/TV	23.9 ± 4.5	23.48	−0.09		18.32	−1.24		
Tb.Th. [μm]	148 ± 23	115.74	−1.40	0.43	107.65	−1.75	0.11	105 ± 25
Tb.N. [1/mm]	1.66 ± 0.22	2.40	3.36	3.50	1.85	0.86	2.10	1.03 ± 0.39
OV/BV [%]	2.12 ± 1.00	15.63	13.51	4.01	7.79	5.67	1.00	5.2 ± 2.6
O.Th. [μm]	6.7 ± 1.7	19.01	7.24	7.95	6.94	0.14	0.85	5.5 ± 1.7
OS/BS [%]	22.1 ± 7.8	60.93	4.98	0.91	80.34	−1.76	2.31	48 ± 14
Ob.S/BS [%]	6.7 ± 4.5	9.21	0.56	−1.07	6.02	−0.71	−1.41	19.4 ± 9.5
Oc.S/BS [%]	0.94 ± 0.38	2.05	2.92	/	0	−2.47	/	1.37 [1.05–1.70]
ES/BS [%]	14.9 ± 5.6	29.70	2.64	/	11.27	−0.65	/	15.6 [13.7 - 21.8]
N.Oc/BS [1/mm]	0.29 ± 0.14	0.45	1.14	−0.06	0	−2.01	−1.62	0.47 ± 0.29
MS/BS [%]	11.7 ± 5.0	16.50	0.96	−0.68	5.40	−1.26	−1.83	23.1 ± 9.7
MAR [μm/d]	0.87± 0.09	1.20	3.67	2.60	1.40	5.89	3.72	0.73 ± 0.18
BFR/BS [$\mu m^3/\mu m^2/y$]	37.3 ± 16.7	72.30	2.09	−0.14	27.60	−0.58	−1.45	77 ± 34

*(Glorieux et al., 2000)

**(Rauch et al., 2000)

#Z-score:

We considered an increase if the value was more than 1 SD above controls/OI i.e. > 1

We considered a decrease if value is more than 1 SD below controls/OI i.e. < -1

We considered normal if value is between -1 and 1

Table 3

BMDD Parameters

BMDD- parameters	Young Reference n=54[a]	Single Control	Diff. [%]	Patient 1	Diff [%]	Patient 2	Diff [%]	α2(I) G190V	Diff [%]	α2(I) G940D	Diff [%]	OI type I n = 19[b]	Diff [%]
CaMean [wt% Ca]	20.95 (0.57)	21.10	0.72	21.56	2.90***	24.07	14.91***	22.81	8.88	22.87	9.16	22.43 (0.63)	7.06
CaPeak [wt% Ca]	21.66 (0.52)	21.84	0.83	23.05	6.41***	25.30	16.81***	23.91	10.39	23.74	9.60	23.39 (0.57)	7.99
CaWidth [Δwt% Ca]	3.47 [3.12;3.64]	3.29	−5.19	4.85	39.77***	3.12	−10.09***	3.64	4.90	3.12	−10.09	3.08 (0.28)	−11.24
CaLow [%]	6.14 [4.95;7.99]	6.27	2.12	11.80	92.11***	5.72	−6.84***	6.47	5.37	4.85	−21.01	5.94 (2.05)	−3.26
CaHigh [%]	0.90 [0.44;1.47]	1.27	42.70	12.72	1329.50***	45.33	4993.10***	18.08	1931.46	10.20	1046.07	7.54 [5.00;11.82]	737.00

Data are mean (SD) or median [25th percentile; 75th percentile]
Diff. = difference to Young Reference

*** p<0.001 versus Young Reference[a] (one-sample t-test and Wilcoxon signed-rank test, correspondingly)

a (Fratzl-Zelman, et al., 2009)

b (Fratzl-Zelman, et al., 2010)